Title: A 3D Extra-Large Pore Zeolite Enabled by 1D-to-3D Topotactic Condensation of a Chain Silicate

Authors: Jian Li[1,2,3]*†‡, Zihao Rei Gao[2,4]†, Qing-Fang Lin[5,6]†, Chenxu Liu[6], Fangxin Gao[5], Cong Lin[2,3,7], Siyao Zhang[5], Hua Deng[8], Alvaro Mayoral[9,10], Wei Fan[11], Song Luo[11], Xiaobo Chen[12], Hong He[8,13], Miguel A. Camblor[4]*, Fei-Jian Chen[5,6]*, Jihong Yu[6]*

Affiliations:

[1]Berzelii Center EXSELENT on Porous Materials, Department of Materials and Environmental Chemistry, Stockholm University; Stockholm, 10691, Sweden.

[2]Anhui ZEO New Material Technology Co.; 778 Dongliu Road, Hefei, 230071, China.

[3]College of Chemistry and Molecular Engineering, Peking University; Beijing, China.

[4]Instituto de Ciencia de Materiales de Madrid, Consejo Superior de Investigaciones Científicas (ICMM-CSIC); c/Sor Juana Inés de la Cruz 3, Madrid 28049, Spain.

[5]Department of Chemistry, Bengbu Medical College; Bengbu, 233030, China.

[6]State Key Laboratory of Inorganic Synthesis and Preparative Chemistry, College of Chemistry; International Center of Future Science, Jilin University; Changchun, China.

[7]Department of Mechanical Engineering, The Hong Kong Polytechnic University; Kowloon, Hong Kong, China.

[8]Center for Excellence in Regional Atmospheric Environment, Key Laboratory of Urban Pollutant Conversion, Institute of Urban Environment, Chinese Academy of Sciences; Xiamen, 361021, China

[9]Instituto de Nanociencia y Materiales de Aragón (INMA), CSIC-Universidad de Zaragoza; Zaragoza 50009, Spain

[10]Laboratorio de Microscopias Avanzadas (LMA-Universidad de Zaragoza); 50018, Zaragoza, Spain

[11]Department of Chemical Engineering, University of Massachusetts; Amherst, MA 01003, USA.

[12]State Key Laboratory of Heavy Oil Processing, China University of Petroleum; Qingdao 266580, China.

[13]State Key Joint Laboratory of Environment Simulation and Pollution Control, Research Center for Eco-Environmental Sciences, Chinese Academy of Sciences; Beijing 100085, China.

*Corresponding author. Email: jxpxlijian@pku.edu.cn (J.L.); macamblor@icmm.csic.es (M.A.C.); feijian@jlu.edu.cn (F.-J.C.); jihong@jlu.edu.cn (J.Y.).

†These authors contributed equally to this work

‡Current address: State Key Laboratory of Coordination Chemistry, School of Chemistry and Chemical Engineering, Nanjing University, Nanjing, 210023 China

Abstract: Zeolites are microporous silicates that find an ample variety of applications as catalysts, adsorbents, and cation exchangers. Stable silica-based zeolites with increased porosity are in demand to allow adsorption and processing of large molecules, but challenge our synthetic ability. We report a novel, highly stable pure silica zeolite, ZEO-3, with a multidimensional, interconnected system of extra-large pores open through windows made by 16 and 14 SiO_4 tetrahedra, which is the least dense polymorph of silica known so far. This zeolite was formed by an unprecedented one-dimensional to three-dimensional (1D-to-3D) topotactic condensation of a chain silicate. With a specific surface area > 1000 square meter per gram, ZEO-3 showed a high performance for volatile organic compounds abatement and recovery compared with other zeolites and MOFs.

One-Sentence Summary: ZEO-3, the most porous stable zeolite known so far, shows potential in volatile organic compounds abatement and recovery.

Main Text:

The size of molecules that can enter, diffuse and react into zeolites are limited by the size of their pores (*1-4*), which are typically described as "of molecular dimensions", actually meaning of the size of small molecules (<7 Å). For many applications, small pores enhance reaction and sorption selectivity (*5*), but for other applications, such as processing large molecules from petroleum or sorption and reaction of organic pollutants, stable zeolites with larger pores are in demand (*6*). Natural and synthetic zeolites possess a fully connected three-dimensional network of corner-sharing SiO_4 tetrahedra; they are tectosilicates or framework silicates (*7*), with Si occasionally substituted by other atoms. However, some zeolites are obtained in the form of two-dimensional precursors (phyllosilicates or layered silicates) (*7*) that only become fully connected tectosilicate zeolites by condensation of their layers through a calcination procedure that is "topotactic" because it does not alter the layer topology (*8-10*). The condensing layers can be obtained by direct synthesis or by disassembly of certain zeolites as in the so-called ADOR (assembly-disassembly-organization-reassembly) process (*11*).

However, after several decades of extensive and systematic zeolite synthesis studies (*12*), there have been no reported examples or predictions of a three-dimensional (3D) zeolite obtained by condensation from a one-dimensional (1D) precursor, either directly synthesized or obtained by disassembly of another zeolite. We report such a 1D-to-3D topotactic condensation from ZEO-2, a directly synthesized complex "zeolitic" chain silicate, into ZEO-3, a fully connected 3D extra-large pore zeolite (ZEO-*n* refers to materials discovered and patented by the Anhui ZEO New Material Technology Co., China). This condensation does not alter the topology of the chain silicate, so it is topotactic. The resulting stable zeolite ZEO-3 exhibits very low density, a multidimensional system of interconnected extra-large pores (Fig. 1), and the presence in its structure of double four-membered ring units (D4R), that is, small cubes of silica. For pure silica zeolites, this kind of unit is strained and up to now was believed to need a fluoride anion near its center to be accessible for crystallization (*13*) because it has never been seen before in a silica zeolite synthesized without the use of F^- anions.

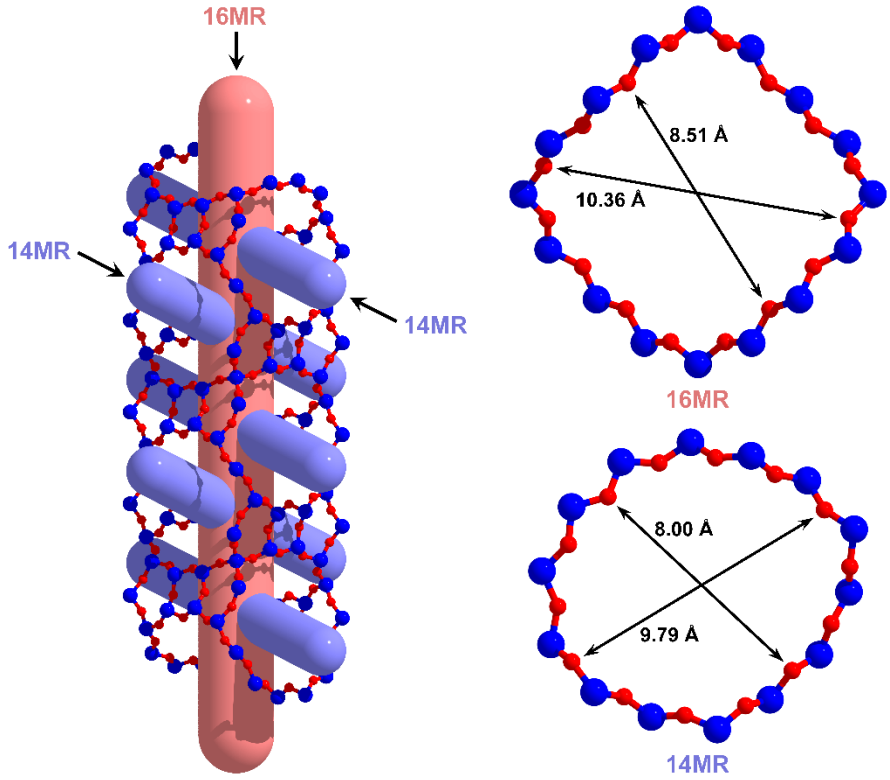

Fig. 1. The extra-large pore system in ZEO-3. The 3D system of interconnected extra-large pore system (left) and the crystallographic pore size of ZEO-3 (right). The van der Waals radius of O (2×1.35 Å) has been subtracted.

Synthesis and structure of the precursor chain silicate

We synthesized the complex chain silica zeolite precursor ZEO-2 using tricyclohexylmethylphosphonium ($C_{19}H_{36}P^+$, tCyMP) as an organic structure directing agent (OSDA) from a gel of molar composition 1 SiO_2 : 0.5 tCyMPOH : 10 H_2O heated at 175 ºC (see Supplementary Material). The structure of ZEO-2 was successfully solved ab initio by using eight continuous rotation electron diffraction (cRED) (*14*) datasets. The pure silicate ZEO-2 crystals display a needle-like morphology (Fig. S1a) and has a *C*-centered monoclinic cell with *a* = 23.5465(7) Å, *b* = 24.7446(7) Å, *c* = 14.4024(4) Å, *β* = 115.1974(9)° (Tables S1 and S2, Fig. S2). ZEO-2 is a complex 1D chain silicate decorated with silanol and silanolate groups (Fig. 2A) that hold the structure together through numerous hydrogen bonds between adjacent chains (Fig. 2, B and C), with the tCyMP cations located in the interchain space (Fig. S5). The cations were occluded intact, as demonstrated by ^{13}C and ^{31}P nuclear magnetic resonance (NMR) (Fig. S6) and amount to 8.85 OSDA per unit cell according to C analysis (25.0 wt%). Hydrogen bonds were observed in the ^{1}H magic-angle spinning (MAS) NMR spectrum as a broad resonance around 15.1 parts per million (ppm) (Fig. S7), indicating a moderate-to-strong hydrogen bond (*15*) corresponding to O···O distances (*16*) of ~ 2.51 Å, in good agreement with the crystallographic distances of 2.47 to 2.52 Å.

The 1D pure silica chains in ZEO-2 are aligned along the [001] direction (Fig. 2A) and surrounded by four identical chains in the *ab* plane (Fig. 2C). At the edge of the ZEO-2 chain, four silanols or silanolates form a single four-membered ring (S4R) that faced, slightly displaced, an identical S4R from the next chain, with hydrogen bonding along the [110] and [1-10] directions connecting adjacent chains (Fig. 2B). The high resolution of the ^{29}Si MAS NMR spectrum of ZEO-2 (Fig. 2D), reveals four Q^3 Si sites (-94.2, -95.8, -98.6, and -100.4 ppm) spanning a chemical shift range unprecedented for Q^3 in zeolites, which are more typically centered at around ~-102±1 ppm). However, the values are well within the general Q^3 range in silicates (*17*). The spectrum also shows seven Q^4 Si sites (from -106.8 to -116.8 ppm) and is thus in good agreement with the crystallographic results (4 Q^3 and 5 Q^4 all with the same multiplicity plus 2 Q^4 with half multiplicity, see Table S5). ^{29}Si{^{1}H} cross polarization (CP) MAS NMR spectroscopy proved the existence of those four Q^3 Si sites in ZEO-2 (Fig. 2D top).

Condensation of 1D chains to 3D-extralarge pore zeolite

Upon calcination in air to remove the OSDA (600 ^{0}C, 3-hour ramp, 6-hour plateau), silanol groups in adjacent chains condensed into Si-O-Si bridges with H_2O elimination, resulting in the pure silica zeolite ZEO-3 (Fig. 3, A-C), which maintained the needle-like morphology (Fig. S1b). The condensation occurred between 370 and 390 ^{0}C (Fig. S8), coincident with the removal of organics (Fig. S15). Phosphorus residues were eliminated by washing with water within an autoclave at 100 ºC for 1 day, or by reduction with H_2 (a mixture of H_2/N_2 with 10/90 volume ratio) from the as-made ZEO-2 sample at 600ºC with a 2-hour ramp and a 6-hour plateau. The structure of ZEO-3 was also solved ab initio by cRED with five datasets (Tables S2 and S3, Fig. S3). The unit cell of ZEO-3 shrank to a = 21.5046(8) Å, b = 21.2757(8) Å, c = 14.4638(4) Å, β = 108.7196(1)° but maintained the same symmetry as ZEO-2, as well as the topology of the chain. Whereas a 17% contraction of the structure occurred along *a*- and *b*- axis, the *c*-axis underwent only a marginal expansion of 0.4%. To obtain more accurate atomic positions, the structures of ZEO-2 and ZEO-3, including the position of the disordered tCyMP in ZEO-2, were subsequently Rietveld refined against synchrotron powder X-ray diffraction data (SPXRD, Figs. S4 and S5, Tables S4 to S10). All the unit cell data given above correspond to the refined structures. The final refined unit-cell compositions of ZEO-2 and ZEO-3 were $[Si_{80}O_{176}H_{24}]|(C_{19}H_{36}P)_8$ and $Si_{80}O_{160}$, respectively (see Supporting Material for details).

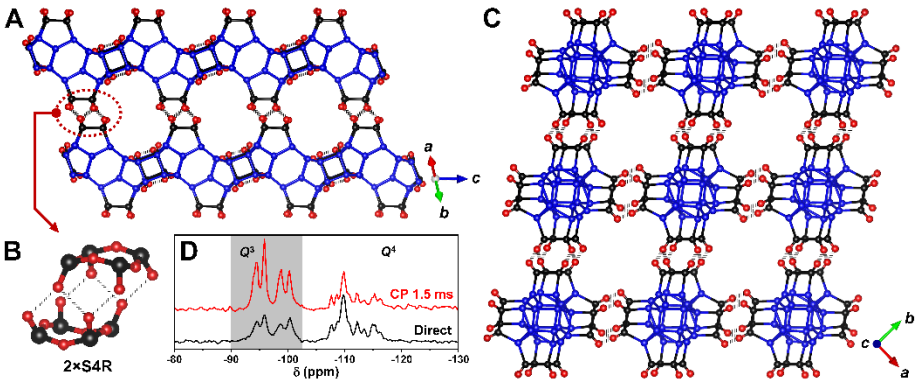

Fig. 2. The structure of the chain silicate ZEO-2. Only O atoms related to the subsequent condensation reaction are shown (small red spheres). Silicon atoms are shown as blue (always Q^4) or black (Q^3 in ZEO-2 converting into Q^4 in ZEO-3). (A) A chain of ZEO-2 is hydrogen bonded (**B**) to four adjacent chains (**C**). (**D**) The ^{29}Si MAS NMR spectrum (bottom) shows resolution of Q^3 and Q^4 silicon sites (4 and 7 sites, respectively). The close proximity of Q^3 sites to H atoms is revealed in the ^{29}Si{^{1}H} CP MAS NMR spectrum by their relative intensity enhanced by polarization transfer from close protons at short contact time (top, 1.5 ms).

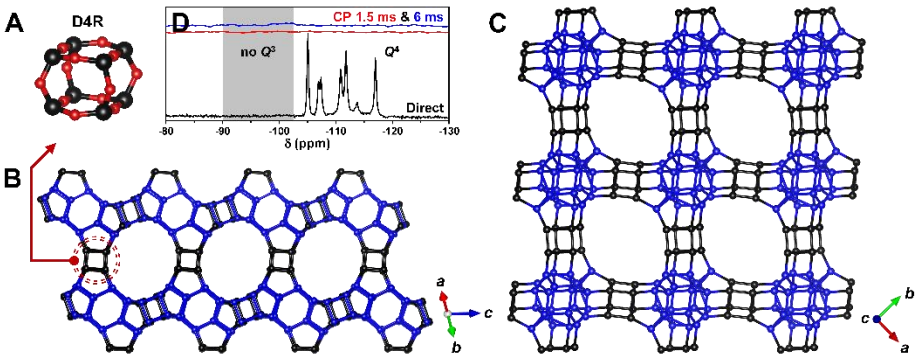

Fig. 3. The 1D-to-3D topotactic condensation into the extra-large pore framework silicate ZEO-3. (**A**) During calcination of ZEO-2, condensation of Q^3 sites through dehydroxylation connects two S4Rs to make a D4R, through which each chain is bonded to four adjacent chains, resulting in the extra-large pore ZEO-3 with 14MR (**B**) and 16MR (**C**) channels. (D) The corresponding ^{29}Si MAS NMR spectra (bottom) is dominated by Q^4 sites with almost no Q^3 defects and hence little intensity enhancement in the ^{29}Si{^{1}H} CP MAS NMR under short (middle, 1.5 ms) or long contact times (top, 6 ms).

During thermal treatment, neighboring S4Rs in ZEO-2 connect to each other to form a D4R (Fig. 3A) by condensation of the terminal Si-OH groups, yielding the fully-connected framework of ZEO-3 (Fig. 3, B and C). The condensed solid is a true, non-interrupted, three-dimensional extra-large pore zeolite. The channel system of ZEO-3 is 3D with 16×14×14 membered-ring (MR) channels (Fig. 3, B and C) and full connectivity between channels (Fig. 1). The fulfillment of the condensation process is demonstrated by the ^{29}Si MAS NMR spectrum of ZEO-3, which reveals total condensation: all Si atoms are Q^4 sites (Fig. 3D, bottom) with a negligible amount of Q^3 that could be assigned to connectivity defects, as proved by the very low intensity enhancement by cross polarization (Fig. 3D middle and top) and FT-IR spectra from self-supported pellets (Fig. S16).

The structural models obtained were fully corroborated by spherical aberration (Cs)-corrected scanning transmission electron microscopy (STEM, Figs. 4 and S10) where a faint signal corresponding to the tCyMP (C and P) was also identified between the chains of ZEO-2 (Fig. 4A) in the place that after condensation will become 14MR pores in ZEO-3. The visualization of ZEO-2 along [001] could not be obtained since it was hampered by the larger thickness (since this is the long needle direction) and the existence in the structure of atoms at different *z* levels that are displaced from one another along *x* and *y*. The 14 and 16 MR pores of ZEO-3 are clearly

visible (Fig. 4, B and C) together with the smaller 4, 5 and 6R in both materials (Figs. 4 and Fig. S10).

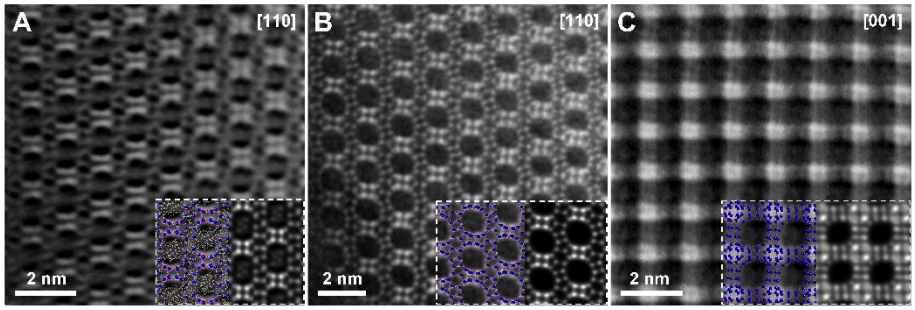

Fig. 4 Cs-corrected STEM visualization of the 1D silicate chain ZEO-2 and 3D zeolite ZEO-3. (A) ZEO-2 along [110] projection, and ZEO-3 showing the extra-large **(B)** 14MR along the [110] and **(C)** 16MR along the [001] projections. All other rings (4Rs, 5Rs and 6Rs) are clearly visible. To facilitate image interpretation, the schematic models (Si atoms in blue and O atoms in red) have been superimposed and the simulated STEM images are also included in the right bottom inset.

The σ expansion of zeolite Beta polymorphs

The details of the topology are shown in Fig. 5 and Tables S11 and S12. The ZEO-2 chain is topologically identical to the one found in polymorph B of zeolite Beta, although in that zeolite it is not an isolated chain but is embedded in the 3D framework. We use here the acronym BEB to refer to that polymorph, although this is not an accepted zeolite topology code. The chain in BEB and ZEO-3 is built by a large composite building unit (CBU, Fig. 5A) that is alternately rotated by +90º and -90º (dotted arrows in Fig. 5B). If the rotation were performed always in the same sense (that is, always by either +90º or -90º, dotted arrows in Fig. 5C) a chiral chain would result, which is in fact embedded in the chiral BEA polymorph of zeolite Beta (space group $P4_122$ or $P4_322$). Thus, condensation of such a chain in a way similar to the condensation of ZEO-2 would result in a new chiral 16×14×14MR hypothetical zeolite. ZEO-3 (Fig. 5D) and this hypothetical chiral zeolite (Fig. 5E) correspond to the σ expansion of polymorphs BEB (Fig. 5F) and BEA (Fig. 5G), respectively, of zeolite Beta (*18*, *19*). A minimization of both structures using the GULP coded suggests the energies of both ZEO-3 and σ-BEA are close to the energy-density relationship normally encountered in zeolites (Fig. S17 and Table S14). Since ZEO-3 has been realized, we believe the hypothetical extra-large pore σ-BEA zeolite might be a reasonable target for future studies.

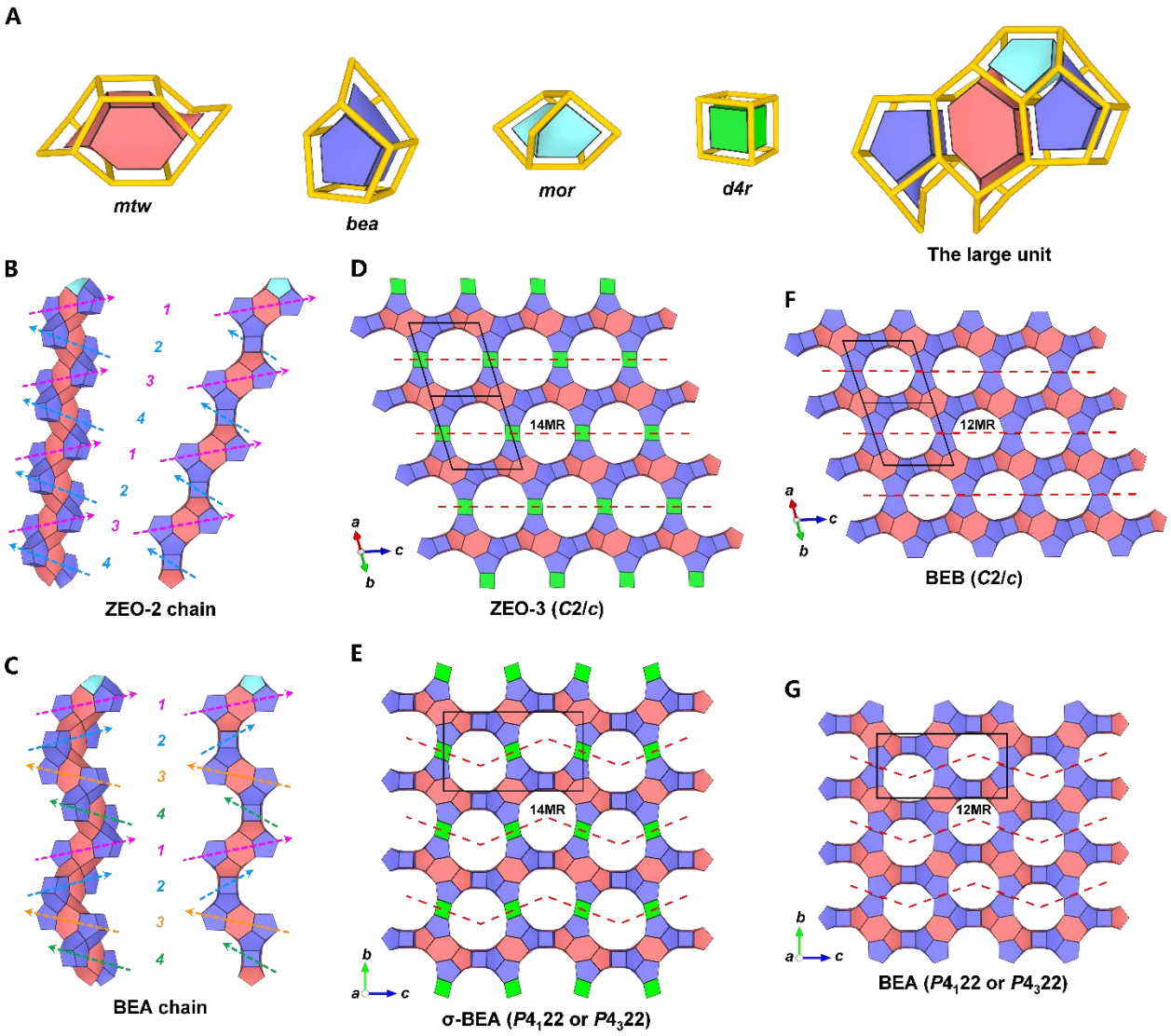

Fig. 5. Topology of ZEO-3 and a hypothetical chiral extra-large pore zeolite. (A) The individual and the large unit CBUs made from them. (**B**) ZEO-2 chain and (**C**) BEA chain built by attaching successive large units, viewed along two different directions. The tiling structures of (**D**) ZEO-3, (**E**) the σ-expanded **BEA**, and polymorphs (**F**) BEB and (**G**) **BEA** of zeolite Beta. Dotted arrows indicate topologically identical large units (units 1, 2, 3, 4) rotated by alternating +90º, -90º, +90º, -90º in **B**, or non alternating +90º, +90º, +90º, +90º, or -90º, -90º, -90º, -90º in **C**. In **D**, **E**, **F** and **G**, the dotted lines separate neighbouring ZEO-2 or BEA chains; in **D** and **E**, the newly formed D4Rs between neighbouring ZEO-2 or BEA chains are highlighted in green; in **F** and **G**, no D4Rs exist as S4R are shared between neighbouring ZEO-2 or BEA chains.

Properties of ZEO-3

ZEO-3 is a stable, fully-connected silicate zeolite containing 3D interconnected pores opened only through extra-large windows. The crystallographic pore sizes of ZEO-3 are 10.36×8.51 Å

and 9.79×8.00 Å for the 16MR and 14MR, respectively (Fig. 1). The 3D extra-large pore nature of ZEO-3 resulted in a very low framework density (FD) value (12.76 tetrahedral atoms, T-atoms, per 1000 $Å^3$). Compared with the other known stable, low density (alumino)silicate zeolites, including **FAU**, **EMT**, ***BEA**, **BEC**, **ISV** and **IWV**, and the recently reported PST-2, PST-32 (*20*), and ZEO-1 (*6*), this value is the lowest and puts ZEO-3 as the crystalline silica polymorph with the most open framework (Table S13). The calculated density of ZEO-3 is just 1.27 g/cm^3, less than half that of quartz (2.65 g/cm^3) and near the density of water.

In fact, ZEO-3 breaks the observed tendency between the framework density and the size of the smallest rings in the zeolite structure (*21*). For an average smallest ring of 4.25, the predicted minimum FD (*21*) is 13 T-atom per 1000 $Å^3$, which is greater than the value for ZEO-3. Compared with the real values of non-interrupted zeolites containing 4- and 5-rings, ZEO-3 is well below the lowest calculated FD of **ISV** and **IWV** (15.0; experimental values of 15.4 and 15.7, respectively).

The observed N_2 and Ar adsorption/desorption isotherms (type Ia) of ZEO-3 revealed high specific surface areas of 989 and 1032 m^2/g (Figs. S11 and S12), respectively. The non-local density functional theory (NLDFT) method applied to the Ar adsorption data calculated mean pore sizes of 10.8 and 8.8 Å (Fig. S13) that match well with the crystallographic results. The extra-large pores of ZEO-3 allowed the diffusion and adsorption of large molecules, like Nile Blue (Fig. S14), suggesting potential for the removal of large organic pollutants from waste liquid streams.

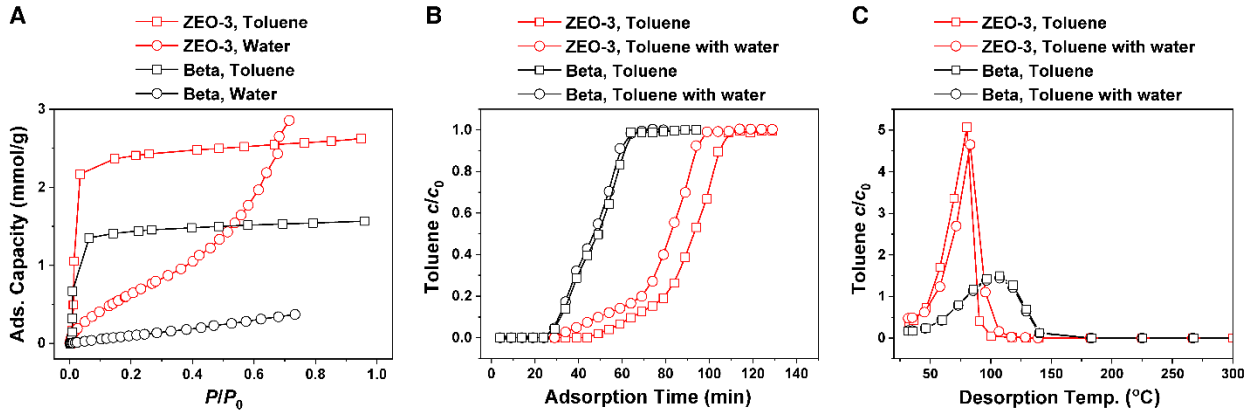

Fig. 6. Application of 3D extra-large pore zeolite ZEO-3 in volatile organic compounds (VOCs) removal. VOCs adsorption isotherms (**A**), breakthrough adsorption (**B**), and desorption curves (**C**) on ZEO-3 (red) and Beta (black) zeolite.

Adsorption has been considered as an energy-saving candidate for volatile organic compounds (VOCs) abatement and recovery (*22*). The development of sorbents with high adsorption capacity, water vapor resistance, and easy regeneration is critical for a successful adsorption technology (*23*). Zeolites are among the best adsorbents for VOCs given their unique microporosity, high adsorption capacity, and non-flammability (*23, 24*). The adsorption equilibrium capacities of toluene and water vapor on ZEO-3 were larger than those on Beta,

which has smaller pores (Fig. 6A). ZEO-3 exhibited much longer breakthrough time (better dynamic capacity) than Beta zeolites with little interference from water (Fig. 6B). The main desorption peak of toluene occurred at a lower temperature for ZEO-3 than for Beta (Fig. 6C) making its thermal regeneration easier. Thus, ZEO-3 outperforms Beta, a reference zeolite for this application (*25, 26*), in terms of adsorption capacity and regeneration potential. Comparison of ZEO-3 with commercial zirconium 1,4-dicarboxybenzene UiO-66, one of the most stable MOFs (*27*), suggested a similar performance for the fresh materials (Fig. S18). However, after recycling the performance of ZEO-3 was maintained whereas that of UiO-66 was compromised. At the end of five adsorption cycles the PXRD pattern of UiO-66 revealed it had been destroyed while ZEO-3 remained stable (Fig. S19). Additionally, the desorption temperature for UiO-66 was significantly higher than that of ZEO-3 (Fig. S20) indicating a poorer regeneration ability. Phosphorous-free ZEO-3 had a high thermal (1100^0C 10^0C/min, 1-hour plateau) and hydrothermal stability (760^0C, 10% H_2O, 3 hours) that may ease its application in real conditions (Fig. S9). It is also possible to introduce active sites (such as Ti) into ZEO-3 through a one-pot synthesis method (Figs. S21-S22). Ultraviolet-visible spectra reveal that Ti-ZEO-3 exhibits both tetra- (~210 nm) and hexa-coordinated (~270 nm) Ti species (Fig. S23). Catalytic properties of Ti-ZEO-3 will be investigated in a future work.

Concluding remarks

Finally, the fact that ZEO-3 presents structural features that sharply depart from previous observations (silica D4R units without F and FD lower than predicted) deserves some consideration. Those previous observations refer to materials directly synthesized by hydrothermal crystallization. The successful synthesis of ZEO-3 demonstrates that materials that may be considered not accessible by direct synthesis can be obtained by post-synthesis transformations, as it has also been observed for zeolites obtained by the ADOR process, which afforded "unfeasible" zeolites (*28*) or the hybrid guest-host pure silica **STW**, which was also predicted unfeasible by direct synthesis (*29*). This observation allows to foresee new materials developed by 1D-to-3D topotactic condensation as it has been the case for the ADOR process. It is worth to mention that the final step in the ADOR process is a 2D-to-3D condensation similar to the 1D-to-3D process reported here but which, however, produces a systematic reduction in pore size with regard to the parent material.

References and Notes

1. J. Zhong, J. Han, Y. Wei, Z. Liu, Catalysts and shape selective catalysis in the methanol-to-olefin (MTO) reaction. *J. Catal*. **396**, 23-31 (2021). doi: 10.1016/j.jcat.2021.01.027.
2. T.-Y. Cui, A. Rajendran, H.-X. Fan, J. Feng, W.-Y. Li, Review on Hydrodesulfurization over zeolite-Based catalysts. *Ind. Eng. Chem. Res*. **60**, 3295-3323 (2021). doi: 10.1021/acs.iecr.0c06234.

3. Y. Wu, B. M. Weckhuysen, Separation and purification of hydrocarbons with porous materials. *Angew. Chem. Int. Ed*. **60**, 18930-18949 (2021). doi: 10.1002/anie.202104318; *Angew. Chem*. **133**, 19078-19097 (2021). doi: 10.1002/ange.202104318.
4. S. Montalvo, C. Huiliñir, R. Borja, E. Sánchez, C. Herrmann, Application of zeolites for biological treatment processes of solid wastes and wastewaters – A review. *Biores. Tech*. **301**, 122808 (2020). doi: 10.1016/j.biortech.2020.122808.
5. M. Dusselier, M. E. Davis, Small-pore zeolites: synthesis and catalysis. *Chem. Rev*. **118**, 5265-5329 (2018). doi: 10.1021/acs.chemrev.7b00738.
6. Q.-F. Lin, Z. R. Gao, C. Lin, S. Zhang, J. Chen, Z. Li, X. Liu, W. Fan, J. Li, X. Chen, M. A. Camblor, F.-J. Chen, A stable aluminosilicate zeolite with intersecting three-dimensional extra-large pores. *Science* **374**, 1605-1608 (2021). doi: 10.1126/science.abk3258.
7. F. Liebau, Nomenclature and structural formulae of silicate anions and silicates. *Structural Chemistry of Silicates*, Springer-Verlag, Berlin, pp. 72 (1985). doi: 10.1007/978-3-642-50076-3_5.
8. L. Schreyeck, P. Caullet, J.-C. Mougenel, J.-L. Guth, B. Marler, A layered microporous aluminosilicate precursor of FER-type zeolite. *J. Chem. Soc. Chem. Commun*. 2187-2188 (1995). doi: 10.1039/C39950002187.
9. R. Millini, G. Perego, W. O. Parker Jr., G. Bellussi, L. Carluccio, Layered structure of ERB-1 microporous borosilicate precursor and its intercalation properties towards polar molecules. *Microporous Mater*. **4**, 221-230 (1995). doi: 10.1016/0927-6513(95)00013-Y.
10. B. Marler, H. Gies, Hydrous layer silicates as precursors for zeolites obtained through topotactic condensation: a review. *Eur. J. Mineral*. **24**, 405-428 (2012). doi: 10.1127/0935-1221/2012/0024-2187.
11. P. Eliášová, M. Opanasenko, P. S. Wheatley, M. Shamzhy, M. Mazur, P. Nachtigall, W. J. Roth, R. E. Morris, J. Čejka, The ADOR mechanism for the synthesis of new zeolites. *Chem. Soc. Rev*. **44**, 7177-7206 (2015). doi: 10.1039/c5cs00045a.
12. C. S. Cundy, P. A. Cox, The hydrothermal synthesis of zeolites: history and development from the earliest days to the present time. *Chem. Rev*. **103**, 663-702 (2003). doi: 10.1021/cr020060i.
13. C. M. Zicovich-Wilson, M. L. San-Román, M. A. Camblor, F. Pascale, J. S. Durand-Niconoff, Structure, vibrational analysis, and insights into host-guest interactions in as-synthesized pure silica ITQ-12 zeolite by periodic B3LYP calculations. *J. Am. Chem. Soc*. **129**, 11512-11523 (2007). doi: 10.1021/ja0730361.
14. M. Gemmi, E. Mugnaioli, T. E. Gorelik, U. Kolb, L. Palatinus, P. Boullay, S. Hovmöller, J. P. Abrahams, 3D electron diffraction: the nanocrystallography revolution. *ACS Cent. Sci*. **5**, 1315-1329 (2019). doi: 10.1021/acscentsci.9b00394.
15. T. Steiner, The hydrogen bond in the solid state. *Angew. Chem. Int. Ed*. **41**, 48-76 (2002). doi: 10.1002/1521-3773(20020104)41:1<48::AID-ANIE48>3.0.CO;2-U.
16. H. Eckert, J. P. Yesinowski, L. A. Silver, E. M. Stolper, Water in silicate glasses: quantitation and structural studies by 1H solid echo and MAS-NMR methods. *J. Phys. Chem*. **92**, 2055-2064 (1988). doi: 0022-3654/88/2092-2055S01.50/0.
17. G. Engelhardt, Multinuclear solid-state NMR in silicate and zeolite chemistry. *TrAC Trends Anal. Chem*. **8**, 343-347 (1989). doi: 10.1016/0165-9936(89)87043-8.

18. R. M. Barrer, *Hydrothermal chemistry of zeolites,* Academic Press, London, pp. 11 (1982).
19. J. V. Smith, Topochemistry of zeolites and related materials. 1. Topology and geometry. *Chem. Rev*. **88**, 149-182 (1988). doi: 0009-2665/88/0788-0149$06.50/0.
20. H. Lee, J. Shin, K. Lee, H. J. Choi, A. Mayoral, N. Y. Kang, S. B. Hong, Synthesis of thermally stable SBT and SBS/SBT intergrowth zeolites. *Science*, **373**, 104-107 (2021). doi: 10.1126/science.abi7208.
21. G. O. Brunner, W. M. Meier, Framework density distribution of zeolite-type tetrahedrals nets. *Nature* **337**, 146-147 (1989). doi: 10.1038/337146a0.
22. M. Li, Q. Zhang, B. Zheng, D. Tong, Y. Lei, F. Liu, C. Hong, S. Kang, L. Yan, Y. Zhang, Y. Bo, H. Su, Y. Cheng, K. He, Persistent growth of anthropogenic non-methane volatile organic compound (NMVOC) emissions in China during 1990-2017: drivers, speciation and ozone formation po-tential. *Atmos. Chem. Phys*. **19**, 8897-8913 (2019). doi: 10.5194/acp-19-8897-2019.
23. C. Yang, G. Miao, Y. Pi, Q. Xia, J. Wu, Z. Li, J. Xiao, Abatement of various types of VOCs by adsorption/catalytic oxidation: A review. *Chem. Eng. J*. **370**, 1128-1153 (2019). doi: 10.1016/j.cej.2019.03.232.
24. S. K. P. Veerapandian, N. De Geyter, J.-M. Giraudon, J.-F. Lamonier, R. Morent, The use of zeolites for VOCs abatement by combining non-thermal plasma, adsorption, and/or catalysis: a review. *Catalysts* **9**, 98, (2019). doi: 10.3390/catal9010098.
25. T. Blasco, M. A. Camblor, A. Corma, P. Esteve, J. M. Guil, A. Martínez, J. A. Perdigón-Melón, S. Valencia, Direct synthesis and characterization of hydrophobic aluminum-free Ti-Beta zeolite. *J. Phys. Chem. B* **102**, 75-88 (1998). doi: 10.1021/jp973288w.
26. Z. Zhu, H. Xu, J. Jiang, H. Wu, P. Wu, Hydrophobic nanosized all-silica Beta zeolite: efficient synthesis and adsorption application. *ACS Appl Mater Interfaces* **9**, 27273-27283 (2017). doi: 10.1021/acsami.7b06173.
27. J. H. Cavka, S. Jakobsen, U. Olsbye, N. Guillou, C. Lamberti, S. Bordiga, K. P. Lillerud, A new zirconium inorganic building brick forming metal organic frameworks with exceptional stability. *J. Am. Chem. Soc*. **130**, 13850-13851 (2008). doi: 10.1021/ja8057953.
28. M. Mazur, P. S. Wheatley, M. Navarro, W. J. Roth, M. Položij, A. Mayoral, P. Eliášová, P. Nachtigall, J. Čejka, R. E. Morris, Synthesis of 'unfeasible' zeolites. *Nature Chem*. **8**, 58-62 (2016). doi: 10.1038/nchem.2374.
29. A. Rojas, M. A. Camblor, A pure silica chiral polymorph with helical pores. *Angew. Chem. Int. Ed*. **51**, 3854-3856 (2012). doi: 10.1002/anie.201108753; *Angew. Chem*. **124**, 3920-3922 (2012). doi: 10.1002/ange.201108753.
30. A. Rojas, E. Martínez-Morales, C. M. Zicovich-Wilson, M. A. Camblor, Zeolite synthesis in fluoride media: structure direction toward ITW by small methylimidazolium cations. *J. Am. Chem. Soc.* **134**, 2255-2263 (2012). doi: 10.1021/ja209832y.
31. Z. R. Gao, S. R. G. Balestra, J. Li, M. A. Camblor, HPM-16, a stable interrupted zeolite with a multidimensional mixed medium–large pore system containing supercages. *Angew. Chem. Int. Ed.* **60**, 20249-20252 (2021). doi: 10.1002/anie.202106734; *Angew. Chem.* **133**, 20411-20414 (2021). doi: 10.1002/ange.202106734.
32. J. D. Gale, A. L. Rohl, The general utility lattice program (GULP), *Mol. Simul.* **29**, 291-341 (2003). doi: 10.1080/0892702031000104887.

33. J. D. Gale, Analytical free energy minimization of silica polymorphs, *J. Phys. Chem. B* **102**, 5423-5431 (1998). doi: 10.1021/jp980396p.
34. K.-P. Schroder, J. Sauer, M. Leslie, C. Richard, A. Catlow, J. M. Thomas, Bridging hydrodyl groups in zeolitic catalysts: a computer simulation of their structure, vibrational properties and acidity in protonated faujasites (H-Y zeolites). *Chem. Phys. Lett*. **188**, 320-325 (1992). doi: 10.1016/0009-2614(92)90030-Q.
35. B. W. H. van Beest, G. J. Kramer, R. A. van Santen, Force fields for silicas and aluminophosphates based on ab initio calculations. *Phys. Rev. Lett*. **64**, 1955-1958 (1990). doi: 10.1103/PhysRevLett.64.1955.
36. S. Smeets, B. Wang, E. Hogenbirk, instamatic-dev/instamatic: 1.7.0. (2021). https://doi.org/10.5281/zenodo.5175957.
37. W. Kabsch, Integration, scaling, space-group assignment and post-refinement. *Acta. Cryst. Sect. D* **66**, 133-144 (2010). doi:10.1107/S0907444909047374.
38. W. Wan, J. Sun, J. Su, S. Hovmoller, X. Zou, Three-dimensional rotation electron diffraction: software RED for automated data collection and data processing. *J. Appl. Cryst.* **46**, 1863-1873 (2013). doi:10.1107/S0021889813027714.
39. G. M. Sheldrick, Phase annealing in SHELX-90: direct methods for larger structures. *Acta Cryst. A* **46**, 467-473 (1990). doi: 10.1107/S0108767390000277.
40. O. V. Dolomanov, L. J. Bourhis, R. J. Gildea, J. A. K. Howard, H. Puschmann, OLEX2: a complete structure solution, refinement and analysis program. *J. Appl. Cryst*. **42**, 339-341 (2009). doi.org/10.1107/S0021889808042726
41. A. A. Coelho, TOPAS and TOPAS-Academic: an optimization program integrating computer algebra and crystallographic objects written in C++. *J. Appl. Cryst*. **51**, 210-218 (2018). doi: 10.1107/S1600576718000183.
42. S. Smeets, L. B. McCusker, C. Baerlocher, S. Elomari, D. Xie, S. I. Zones, Locating organic guests in inorganic host materials from X-ray powder diffraction data. *J. Am. Chem. Soc.* **138**, 7099-7106 (2016). doi:10.1021/jacs.6b02953.
43. M. W. Deem, R. Pophale, P. A. Cheeseman, D. J. Earl, Computational discovery of new zeolite-like materials. *J. Phys. Chem. C* **113**, 21353-21360 (2009). doi: 10.1021/jp906984z.
44. T. Blasco, M. A. Camblor, A. Corma, J. Pérez-Pariente, The state of Ti in titanoaluminosilicates isomorphous with zeolite Beta, *J. Am. Chem. Soc*. **115**, 11806-11813 (1993). doi: 10.1021/ja00078a020.
45. Cambridge Crystallographic Data Center (CCDC), structure ICSD-153453. http://www.ccdc.cam.ac.uk.
46. M.-J. Díaz-Cabañas, P. A. Barrett, M. A. Camblor, Synthesis and structure of pure SiO2 chabazite: the SiO2 polymorph with the lowest framework density. *Chem. Commun*. 1881-1882 (1998). doi: 10.1039/A804800B.
47. R. F. Lobo, M. E. Davis, CIT-1: a new molecular sieve with intersecting pores bounded by 10- and 12-rings. *J. Am. Chem. Soc.* **117**, 3766-3779 (1995). doi: 10.1021/ja00118a013.
48. L. A. Villaescusa, P. A. Barrett, M. A. Camblor, ITQ-7: a new pure silica polymorph with a three-dimensional system of large pore channels. *Angew. Chem. Int. Ed.* **38**, 1997-2000, (1999). doi: 10.1002/(SICI)1521-3773(19990712)38:13/14<1997::AID-ANIE1997>3.0.CO;2-U.

49. M. A. Camblor, A. Corma, P. Lightfoot, L. A. Villaescusa, P. A. Wright, Synthesis and structure of ITQ-3, the first pure silica polymorph with a two-dimensional system of straight eight-ring channels. *Angew. Chem. Int. Ed. Engl.* **36**, 2659-2661 (1997). doi: 10.1002/anie.199726591.
50. A. Cantín, A. Corma, M. J. Diaz-Cabanas, J. L. Jordá, M. Moliner, Rational design and HT techniques allow the synthesis of new IWR zeolite polymorphs. *J. Am. Chem. Soc.* **128**, 4216-4217 (2006). doi: 10.1021/ja0603599.
51. C. Baerlocher, L. B. McCusker, Database of zeolite structures, http://www.iza-structure.org/databases/.
52. B. W. Boal, J. E. Schmidt, M. A. Deimund, M. W. Deem, L. M. Henling, S. K. Brand, S. I. Zones, M. E. Davis, Facile synthesis and catalysis of pure-silica and heteroatom LTA. *Chem. Mater.* **27**, 7774-7779 (2015). doi: 10.1021/acs.chemmater.5b03579.
53. M. A. Camblor, A. Corma, M.-J. Díaz-Cabañas, C. Baerlocher, Synthesis and structural characterization of MWW type zeolite ITQ-1, the pure silica analog of MCM-22 and SSZ-25. *J. Phys. Chem. B* **102**, 44-51 (1998). doi: 10.1021/jp972319k.

Acknowledgments: We thank Dr. Carlos Márquez (ICP-CSIC) for the FT-IR measurements, Dr. Risheng Bai (JLU) for his kind suggestions in the synthesis and characterization on the titanosilicate ZEO-3, M. J. de la Mata (SIdI-UAM) for her expedited help in collecting MAS NMR spectra, and Dr. Agnieszka Ziolkowska (Umeå University) for her help in TEM sample preparation by ultramicrotomy.

Funding: Financial support from the National Natural Science Foundation of China (grant numbers: 22288101, 21920102005, 21835002, 22271115, 21601004, 21621001, 21776312, 22078364), the National Key Research and Development Program of China (Grant numbers: 2022YFA1503600, 2021YFA 1501202), the 111 project (B17020), the Natural Science Foundation of the Higher Education Institutions of Anhui Province, China (grant numbers: KJ2020A0585), and the Spanish Ministry of Science Innovation (PID2019-105479RB-I00 project, MCIN/AEI/10.13039/501100011033, and RYC2018-024561-I, Spain) is gratefully acknowledged. The cRED data were collected at the Electron Microscopy Center (EMC), Department of Materials and Environmental Chemistry (MMK) in Stockholm University with the support of the Knut and Alice Wallenberg Foundation (KAW, 2012-0112) through the 3DEM-NATUR project. Use of the Advanced Photon Source at Argonne National Laboratory was supported by the U. S. Department of Energy, Office of Science, Office of Basic Energy Sciences, under Contract No. DE-AC02-06CH11357. Additional funding from the European Union's Horizon 2020 research and innovation program under grant agreement No 823717 - ESTEEM3 and the regional government of Aragon (DGA E13_20R) is also acknowledged.

Author contributions: F.-J.C. conceived the project. J.L., M.A.C., F.-J.C., and J.Y. supervised this work. Z.R.G., Q.-F.L., C.L. (Liu), F.G., S.Z., and F.-J.C. performed the synthesis work. J.L. solved the structure and performed Rietveld refinement and framework energy calculations. Z.R.G. analyzed the topology. J.L., Z.R.G., C.L. (Liu), C.L. (Lin), W.F.,

S.L., X.C., and M.A.C. carried out the physicochemical characterization. H.D. worked on the VOCs application. A.M. performed the HRSTEM tests. M.A.C. prepared the initial draft. J.L., W.F., M.A.C., F.-J.C., and J.Y. organized the work and the draft. All the authors discussed the results and revised the manuscript.

Competing interests: J.L., Q.-F.L., Z.R.G., C.L., and F.-J.C. have filed a patent on zeolites ZEO-2 and ZEO-3. J.L., Z.R.G., and C.L. are affiliated with the company holding the rights on that patent.

Data and materials availability: The datasets generated during and/or analyzed during the current study are available from the corresponding authors on reasonable request. Crystallographic parameters for the structure of ZEO-2 and ZEO-3 refined against SPXRD and cRED data are archived at the Cambridge Crystallographic Data Center (www.ccdc.cam.ac.uk/) under reference Nos. CCDC 2125815-2125816 (SPXRD data) and CCDC 2125677-2125678 (cRED data).

Supplementary Materials

Materials and Methods

Supplementary Text

Figs. S1 to S23

Tables S1 to S14

References (*30*–*53*)